Electrochemical Roughening and Carbon Nanotube Coating of Tetrodes for Chronic Multitarget Neuronal Recordings

Zifeng Xia[1,2], Gonzalo Arias-Gil[1,2], Martin Deckert[3], Maike Vollmer[1,4], Andrew Curran[1,4], Rodrigo Herrera-Molina[1,5], Marcel Brosch[1,2], Kristine Krug[1,2,6], Bertram Schmidt[3], Frank W. Ohl[1,2], Michael T. Lippert[1], and Kentaroh Takagaki*[1,2]

[1]Leibniz Institute for Neurobiology, Magdeburg
[2]Institute for Biology, Otto-von-Guericke University Magdeburg
[3]Institute of Micro- and Sensor Systems, Otto-von-Guericke University, Magdeburg
[4]Department of Otolaryngology-Head and Neck Surgery, University Hospital Magdeburg, Otto von Guericke University, Magdeburg
[5]Centro Integrativo de Biología y Química Aplicada, Universidad Bernardo OHiggins, Santiago, Chile
[6]Department of Physiology, Anatomy and Genetics, Oxford University, Oxford UK

May 29, 2020

Abstract

Stable recordings are a precondition to understanding the fundamental role of long-term brain processes involved in neural plasticity, learning, pathogenesis, and aging. Despite recent advances in materials engineering, digital signal acquisition, and analysis algorithms, stable recording from isolated neurons over longer periods of time remains a challenge. In this study, we combined advances in material chemistry and surgical technique to develop a "Magdeburger" multi-tetrode array that enables parallel recording of multiple single-neurons with long-term signal stability and high signal-to-noise ratio at a reasonable cost. Flexible platinum-iridium tetrodes were electrochemically roughened and coated with carbon nanotubes, thereby decreasing electrode impedance and increasing charge transfer. Packaging of multi-tetrode arrays, tetrode rigidity, and insertion techniques were optimized to minimize tetrode tip movement and to allow simultaneous recordings from independently targeted brain regions even at greater depths in both rodents and primates. Together, the Magdeburger probe provides a basis for a wide range of experimental and translational approaches that require long-term-stable and simultaneous high-quality recordings across different structures throughout the mammalian brain. Areas of potential application include cognitive learning and memory, aging, pathogenesis, neural correlates for behavioral performance, and the development of neuronal brain-computer interfaces for humans.

Currently, four main classes of electrodes are standard for chronic in vivo recordings of neural activity: microwire arrays, Utah arrays, silicon probes, and flexible thin polyimide-based electrodes [1]. These electrodes were designed primarily to record from as many units (neurons) in the brain as possible, but they suffer from long-term instability and usually cause significant cortical thinning or fibrotic changes that develop over several months. Therefore, long-term stable juxtacellular recordings obtained simultaneously from different structures and depth across the mammalian brain still remain a challenge.

Microwire arrays are made of insulated sharpened metals, packaged in brush- or comb-like arrays [2,3,4]. In very exceptional cases, these electrodes can demonstrate stable single unit recordings over months [3,4]. More

recently, solid-state-based versions of such a thin-wire brush approach have been proposed [5,6,7]. The smaller diameter of these solid-state microwires minimizes tissue damage, but their flexibility in the transverse direction limits the accuracy of positioning individual electrode tips [5,6,7]. Moreover, the propulsive implantation procedure most commonly used precludes recording from deep areas in both rodent and primate brain.

Utah arrays are silicon-based microelectrode arrays with 96 contacts. They are the most popular implant for chronic recordings in primates (including humans) and allow single-unit recordings and stimulation with high spatial resolution [8,9]. However, standard Utah arrays are limited to a penetration depth of 1.5 mm [10] and are, therefore, not suitable for recordings from deeper regions within the mammalian brain. Furthermore, the fixed geometry does not allow individually-targeted multisite recordings. More fundamentally, limited biocompatibility leads to encapsulation and cortical thinning after several months of implantation [10,11,12,13,14]. Also, each neuron is only recorded from a single microelectrode contact, and long-term spike identification cannot benefit from the sorting precision provided by narrow-spaced multitrode sampling [15,16,17].

Silicon shaft probes have addressed the targeting of deeper structures in rodent brain and consist of many recording contacts, often packed into small areas [18]. Hundreds of units can be recorded from a single insertion, but unit waveforms tend to "drift" over time and fail to achieve long-term stability. Flexible thin-film probes can be implanted into deeper areas of the primate brain, and mitigate the problem of drift [19,20,21]. Implantations of a few probes can be scaled up to larger numbers using an automated sewing-machine like approach [22]. However, the smoothness of these electrodes relative to their axial rigidity is not conducive to chronic anchoring within the pulsating brain, and chronic tracking of equivalent unit waveforms has not been reported. In summary, despite significant advances, current approaches do not satisfy the needs of modern clinical and translational neurophysiology. Namely, they fail to reliably ensure chronic recordings from the same identified units, especially in deeper areas of the primate brain.

The remaining engineering challenges can be grouped conceptually into two classes: mechanical flexibility and size-impedance tradeoff.

With respect to mechanical flexibility, a balance must be struck between two contradicting requirements: flexibility to allow pulsation together with brain tissue on the one hand, and sufficient rigidity to enable low-trauma targeted implantation to deep areas on the other hand. Current approaches to striking such a balance are to insert very soft electrodes via a thin carrier needle [19,20] or to inject them propulsively under pressure [5,6,7,23]. These approaches reduce insertion trauma but suffer from long-term instability and limited accuracy in targeting specific brain regions. Injection-based approaches are currently optimized for superficial rodent cortex, and they fail to reach deeper areas of the primate brain. We address this issue by choosing a direct implantation approach with our "Magdeburger" probe, which is composed of axially rigid but transversely flexible soft platinum-iridium (Pt-Ir) wire tetrodes. The wire thickness of 25-30 µm is optimized to guarantee the desired mechanical properties and spatial sampling.

Recordings from twisted tetrode packages allow fundamentally more precise sorting of signals from different neighboring neurons when compared to classic single contact recordings [15,16]. For our tetrode packaging, wires with several diameters were tested with and without heat curing. Implantation stability was screened with mock-surgical deep penetrations into semi-transparent 0.65% agarose gel, which is known to model the firmness of mammalian brain [24]. Pt-Ir wires with a thickness of 25-30 μm were chosen due to their ease of mechanical handling during surgery. Thinner Pt-Ir wires were too flexible for direct implantation, and nickel-chromium (NiCr) wires which are also often used for tetrode manufacture were too rigid for direct stable implantation into the pulsating brain.

The second remaining challenge with respect to electrode contact size is to balance geometric compactness and low impedance. Geometric compactness is needed to isolate action potential signals from single neurons and distinguish them from nearby neurons. Although a smaller contact area results in higher impedance, a low impedance is required to achieve a high signal-to-noise ratio recording. High signal-to-noise ratio is especially important in the awake cortex where local field potentials can manifest as high-amplitude fast spike-like signals, whereas low amplitude firing from distal units can easily be obscured by noise.

Various materials and nanomaterials have been tested to lower the impedance of microelectrode contacts. These include gold plating [25,26], carbon nanotube coating [27,26], and PEDOT coating [28]. However, these coatings have not achieved wide acceptance in neurophysiology, due to difficulties in the manufacturing process and problems with coating stability *in vivo*. Coating stability problems are particularly pronounced in packages such as sharp tungsten electrodes, Utah arrays, and side-contact silicon probes, because axial advancement during implantation leads to shearing force in the delaminating direction. We addressed this challenge by developing a synergic electrochemical roughening/carbon nanotube coating procedure that leads to a two-orders-of-magnitude decrease in impedance relative to the native wire and a one-order-of-magnitude decrease compared to state-of-the-art materials and coatings. This allowed us to minimize electrode noise (usually the limiting factor in such recordings) and to approach the amplifier noise levels of current neural amplifiers. Importantly, as documented below, our coating is resistant to the aforementioned implantation shear.

For electrochemical roughening, tetrodes were immersed in 0.5 M sulfuric acid solution, and a train of electrical square wave pulses was applied for several minutes (see Methods and Supplementary Fig. 2). After roughening (Fig. 1a, lower left), sponginess at the sub-micron level is evident compared to the native cut surface (Fig. 1a, upper left). During the development of our protocol, we found that fine adjustments of roughening time and the use of sonication to avoid gas buildup were key factors in order to prevent destructive changes of the electrode surface (Supplementary Figs. 1, 2). This roughening of the electrode surface reduced contact impedances that were well over an order of magnitude lower than the impedances of the original cut electrodes (Fig. 1b). Furthermore, roughening led to a slight increase in charge transfer capacity (Fig. 1c), whereby a stable ionic microenvironment at the electrode tip allows more directed neuronal recordings with less electrode drift [29]. Subsequent carbon nanotube electroplating of the roughened surface led to an additional decrease in electrode impedance of approximately two orders of magnitude when compared to the native wire (Fig. 1b) and further improved charge transfer capacity (see Fig. 1c and Methods). Impedance spectroscopy showed a log-linear decline over the range of neuronal-spike-relevant frequencies, indicating a predominantly capacitive electrode interface (Supplementary Fig. 4). Acute implantation of these ultra-low impedance flexible Magdeburger probes led to recordings of high signal-to-noise ratio unit signals in both rodent and primate brain (Fig. 2).

It should be noted that initial ramping of coating voltage proved to be critical (Supplementary Fig. 3). Ramping did not change electron-micrographic surface appearance or ohmic characteristics, but prevented crosslinking and led to overall improvement in coating stability during and immediately after implantation (Supplementary Fig. 3, Supplementary Table 5).

Packaging and surgical approach were also critical to achieving atraumatic implantation and stable chronic multi-parallel single unit recordings. The most successful approaches to date for recording from clearly isolated single units while maintaining stable waveforms over several weeks have been based on thin and flexible microwires [3,30,5,4,23]. This approach is stable presumably because the thin microwires move flexibly with brain micromovements and pulsation, thereby keeping the tip in a stable position relative to the recorded units. Moreover, microwires can be inserted without a carrier, thus, reducing the risk of tissue damage and scarring. However, penetration into deep brain areas remains a fundamental issue, especially for silicon-based propulsive injection approaches [5,23].

Tetrodes and other electrode configurations have recently regained interest for chronic unit isolation [17,31]. Compared to signals from a single contact, the four channels of a tetrode allow fundamentally more precise sorting by providing four semi-independent measurements and more degrees of freedom that lead to a better measure of unit identity especially when waveforms drift. Moreover, the spatial information in tetrode recordings and differentiation from noise allow unambiguous recording from subcellular extracellular signals, such as dendritic spikes [32].

In order to achieve a carrier-less surgical approach, we designed a 3D-printed polylactic acid tetrode holder that stably holds the tetrodes and allows axial insertion without transverse deformation or bending (Fig. 3e). Anatomically, the rodent skull is significantly more plastic than the primate skull, often with open cranial

sutures well into adulthood. This poses a difficulty when mounting electrode assemblies for chronic recordings. Conventional high-channel-count connectors, such as those available from Omnetics, are designed to have particularly high stability, but require non-negligible insertion force. Moreover, a typical neurophysiological plug package is mounted perpendicularly on the animals' heads and applies perpendicular force to the dorsal surface of a rodent skull leading to dorsoventral skull or brain deformation during plug insertion and removal. To avoid the risk of such deformation, we have designed a laterally-oriented low-insertion-force Hirose DF12 board-to-board plug and tetrode holder package (Fig. 3b, c). The plug is stabilized by a custom 3-D printed clip (Fig. 3f). Another advantage of this connector strategy is the cost-effectiveness. The Hirose plugs are available in the 10-20 Euro cent range, compared to the 100 Euro range for conventional plugs. This package also allows effective mounting of other electrode types on the rodent skull.

Carbon nanotube *in vivo* electrodes have not been commercialized, and have only been used rarely to date [27,26,33], primarily because of four factors: fickleness of the coating process, instability of prior coatings, easy shearing (discussed above), limited shelf life, and limited stability in solution (Sherman Wiebe, personal communication). We evaluated the shelf life of our coating over the course of one year by conducting longitudinal impedance measurements in 3 M potassium chloride (KCl) solution. We found that our coating maintains stable impedances for over one year, which is compatible with commercialization of batch-manufactured lots (Fig. 4a). It is also of interest that the impedances of the electrode contacts themselves were significantly more stable than the impedances of unwanted crosslinks between tetrode contacts—the the latter showed increases in impedances of up to one order-of-magnitude over the same year of measurement (Fig. 4b). As unwanted crosslinks tend to rise in impedance during shelf storage, coating protocols for mass production may be biased toward achieving the lowest possible impedances and accepting a certain level of overcoating, since any accidental crosslinking from overcoating will be eliminated during shelf storage, without affecting the quality of signal separation.

In the past, several groups have reported single unit recordings from isolated neurons over several months, especially in primates [3,34,4,17]. Other groups have reported cases of long-lasting unit recordings from rodents [30]. However, no group to date has been able to juxtacellularly record from a large number of clearly identifiable units for extended periods of time. Using our Magdeburger tetrodes, we were able to stably record from various regions in the rodent and monkey brain with high signal-to-noise ratios (Fig. 2a, c-d, Fig. 5g). For validation purposes, we focused here on signals from juxtacellular recordings. Juxtacellular recordings are defined as unit recordings with very large amplitude waveforms recorded from neurons that are presumably adjacent ("juxta") to the electrode tip [35]. The regular occurrence and stability of these juxtacellular recordings in our preparation (Fig. 5) is remarkable, because we did not intentionally target them as the usual procedure for juxtacellular recordings with glass electrodes [35]. Instead, we believe that our juxtacellular signal developed over the course of several weeks of post-surgical recovery by biological mechanisms. The interface biocompatibility of our coating may be permissive to neural outgrowth and direct contacting of neuron processes onto electrode contacts (Supplementary Fig. 9), resulting in fortuitous juxtacellular arrangements arising several weeks after implantation (Fig. 5). This juxtacellular arrangement allowed signal-to-noise ratios approaching those of intracellular recordings, but with a less invasive extracellular recording configuration (Fig. 5) [35]. In our approach, such juxtacellular recordings were stable for weeks instead of the usual hours (Fig. 5). We regularly check post-mortem histology, and following successful long-term recordings, we did not observe any neuropathology such as gliosis and atrophy. Although it is fundamentally impossible to prove a negative observation, the lack of histological pathology is supportive of the contention that our biomicroengineering and material engineering approaches are enabling favorable long-term biocompatibility.

In summary, the Magdeburger multi-tetrode array allows robust chronic neuronal recordings from various regions and different depths in both rodent and primate brains. Such stable recording conditions were due to various factors. First, we selected a soft metal substrate that provided high tetrode flexibility in the transverse direction and, at the same time, allowed implantation without the need of a carrier or a head-mounted electrode drive. The long-term signal stability from single neurons indicates that the tetrodes were anchored in the tissue, likely by the micro-contour of the twisted electrode shank. Second, we developed

an electrochemical roughening procedure and synergic carbon nanotube coating procedure, which lowered the impedance of the electrodes to the sub 10 kOhm range with a large charge transfer capacity. The low-impedance microsurface was fractal at the molecular-scale but was nonetheless mechanically stable during implantation and offered a long shelf life. The coating of the electrodes also proved biologically favorable characteristics, allowing proximal neurite outgrowth and juxtacellular unit recordings of high signal-to-noise quality. In contrast to other chronic electrode implants, long-term neuropathological changes that could preclude widespread experimental and translational use were not observed. Moreover, the described package allows independent targeting of multiple brain regions. Accessibility of regions at greater depths highlights the applicability of the new tetrode array for recordings even in larger brains, including those of non-human primates and humans, as well as in rodents.

We think that the present advances in electrode design will be of significant interest to neuroscientists in investigating the behavioral physiology of various areas and to translational neurologists who are concerned with the attributes of long-term neural plasticity that underlie behavioral performance, learning and memory. Furthermore, we believe that the characteristics of the Magdeburger probe provide a safe and suitable basis for the development of future human brain-computer interfaces.

Figures

Figure 1 | Characterization and comparison of various electrode surfaces. a, Electron-microscope images of tetrode contacts with variable surface processing: cut/untreated (∅, top-left), coated with carbon nanotubes (CNTs) (C, top-right), electrochemically roughened (R, bottom-left), and electrochemically roughened and CNT coated (R+C, bottom-right). Scale bars: 10 µm, insets 5x magnification. **b**, Impedances of tetrode contacts with various surface processings: cut/untreated ([?],650-900 kOhm,upper and lower quartiles), CNT coated (C, 8-15 kOhm), roughened (R, 8-19 kOhm), roughened and CNT coated (R+C, 4-6 kOhm). **c**, Cyclic voltammetry scan of differently processed tetrodes, as described in main text.

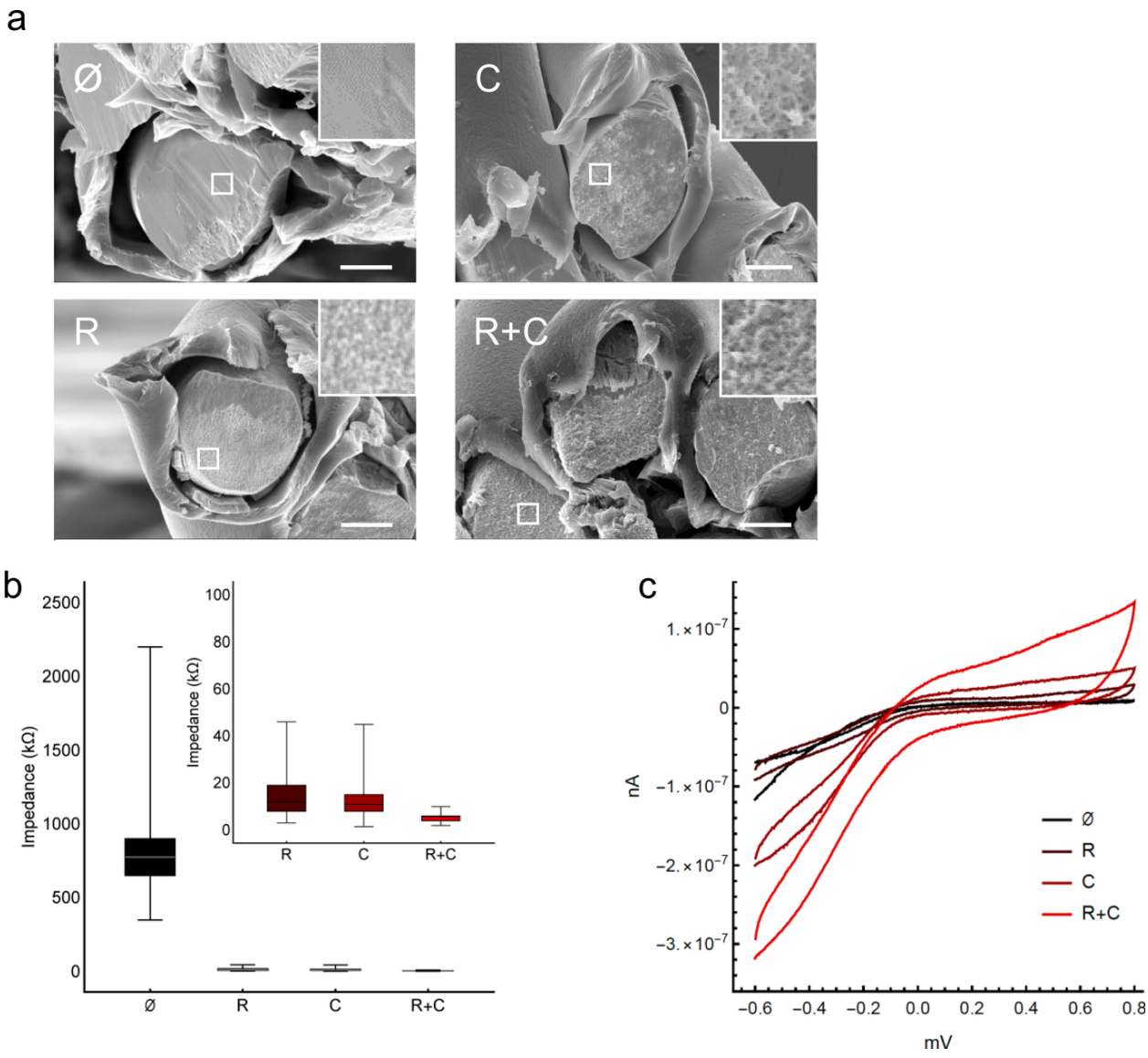

Figure 2 | Effect of roughening and carbon nanotube coating on signal-to-noise ratio. a, Example traces from acute recordings in the globus pallidus externus of the rat obtained with four different contact preparations. Scale bars x/y: 100 ms/100 μV. Although both cut and roughened contacts showed unit spiking, the signal-to-noise ratio was low ([?] and R). Unit signals with larger signal-to-noise ratio were seen with coated tetrode preparations (C, and R+C). Abbreviations for the conditions are as described in legend to Fig. 1a. **b**, Number of units detected in acute globus pallidus externus recordings per tetrode for the four different contact preparations. Recordings were made acutely after implantation. Higher unit count was obtained with carbon nanotube coated contacts (C, R+C). Boxes denote quartiles, horizontal bar is median, whiskers denote most extreme outliers. **c**, Representative acute traces recorded from area 46 in a rhesus macaque. Scale bars x/y: 100 ms/100 μV. Data are clipped to display low-amplitude activity, see d for full scale. **d**, Boxed segment in c, at lower magnification. Scale bars x/y: 10 ms/250 μV. Clear juxtacellular recordings of a bursting unit, approximately 500 μV in amplitude. The high signal-to-noise ratio suggests the potential for translation to chronic implantation in the primate cortex where such unit isolation is usually not possible nor stable.

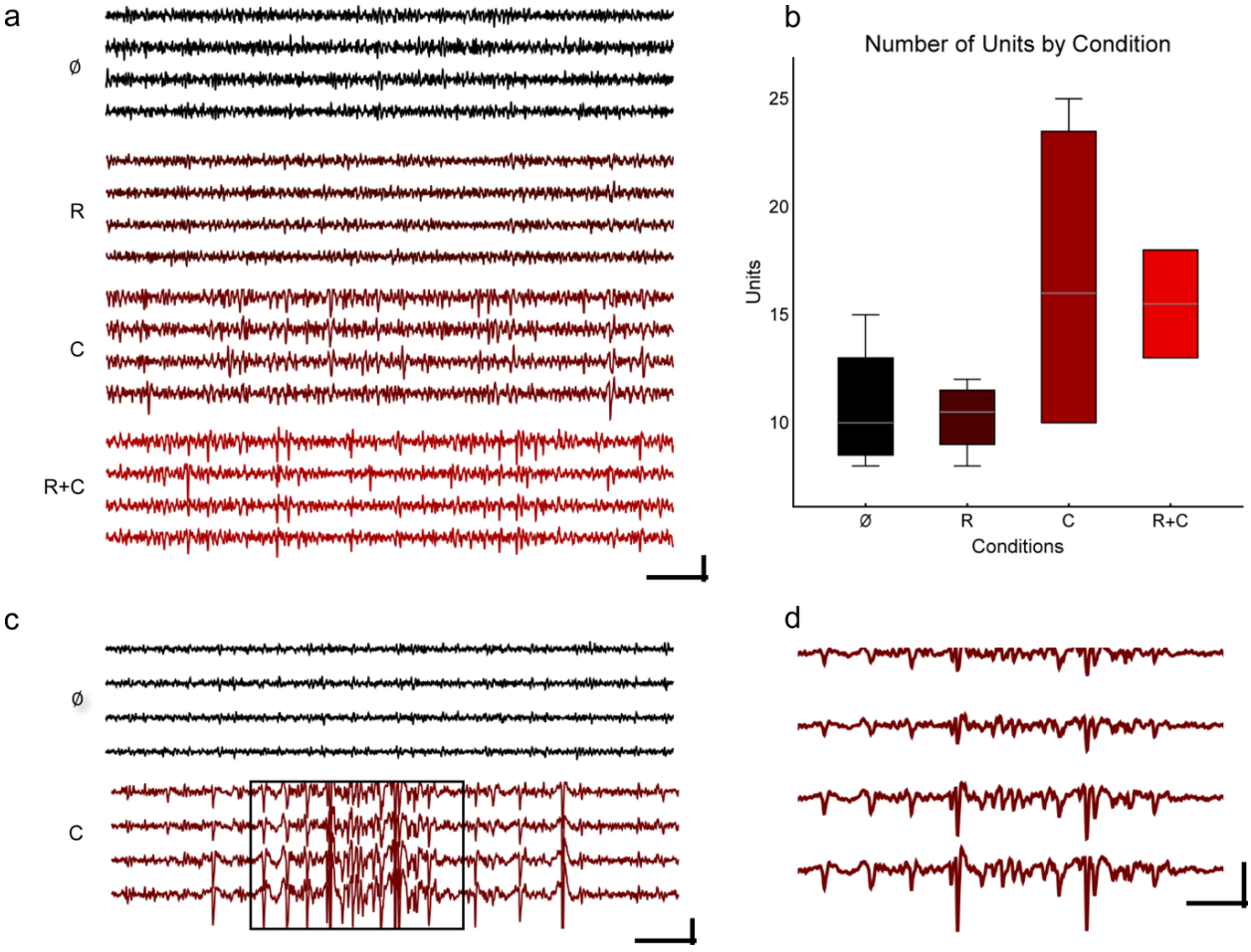

Figure 3 | Technical setup and engineering for manufacture and low-trauma implantation of roughened and coated tetrodes. **a**, Electron micrograph of a micromanufactured twisted tetrode, polished with a circular grinder to 90 degrees at the tip. **b**, A custom circuit board serves as an implantable contact interface for flexible tetrodes. The board consists of 32 gold plated contact holes for eight tetrodes, 4 gold plated holes for reference electrodes (Ref 1-4), and 2 gold plated holes for ground electrodes. **c**, Sample implant with tetrode circuit board (Fig. 3b.), ground electrodes, chlorided reference electrodes, and 8 roughened and carbon nanotube coated tetrodes mounted with gold pins. Scale bar: 10 mm. **d**, Experimental setup for tetrode carbon nanotube coating. A voltage of +550 mV is applied to each electrode individually. **e**, A 3D-printed custom electrode holder for holding and driving of tetrodes during implantation. Scale bar: 5 mm. **f**, A 3D-printed clip to temporarily attach the circuit board and the headstage for mechanical stability. Scale bar: 5 mm.

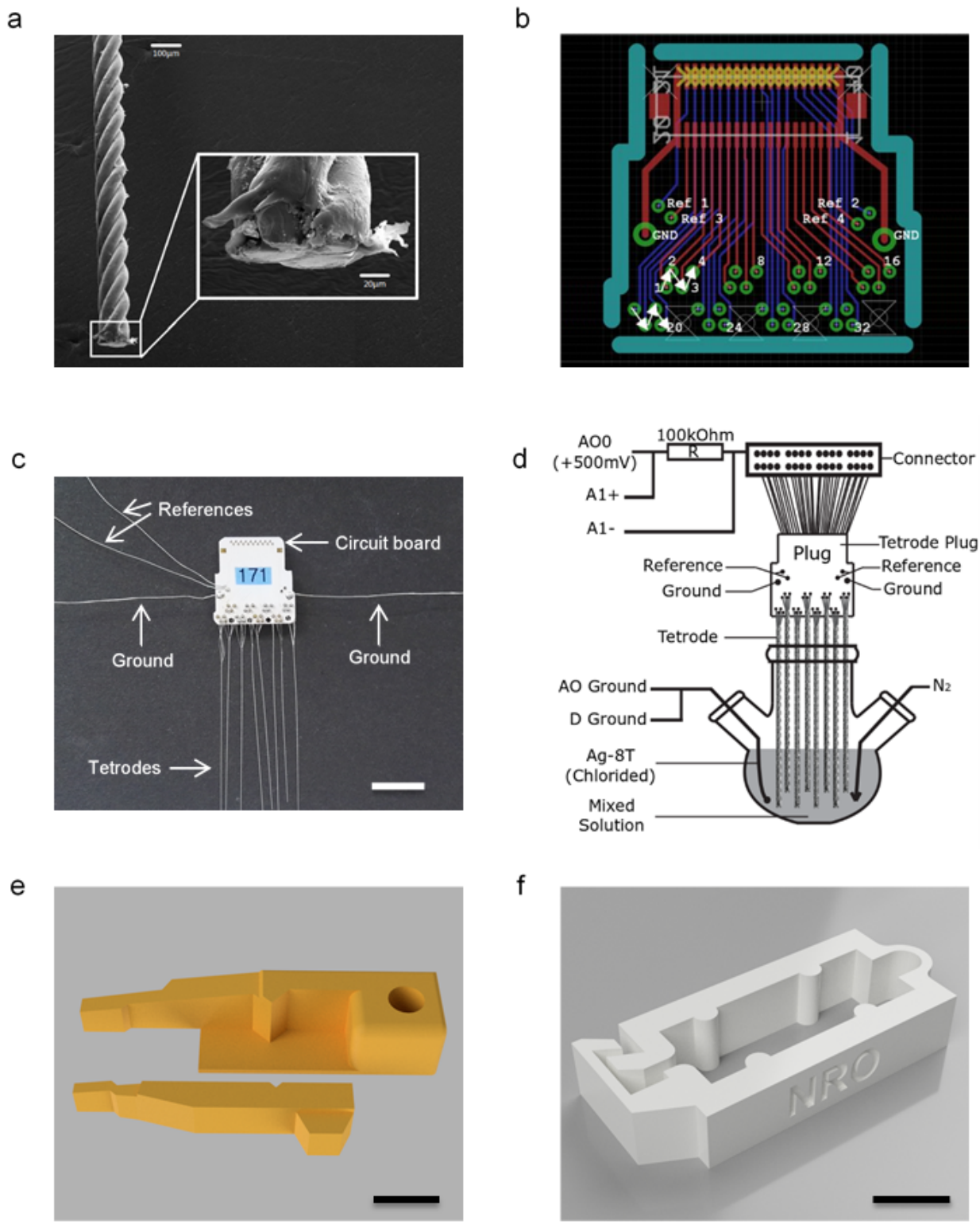
a
b
c
d
e
f
100μm
20μm
Ref 1
Ref 3
Ref 2
Ref 4
GND
GND
2
4
8
12
16
1
3
20
24
28
32
References
Circuit board
171
Ground
Ground
Tetrodes
AO0
(+500mV)
100kOhm
R
Connector
A1+
A1-
Plug
Tetrode Plug
Reference
Ground
Reference
Ground
Tetrode
AO Ground
D Ground
N2
Ag-8T
(Chlorided)
Mixed
Solution
NRO

Figure 4 | Shelf life of carbon nanotube coating. a, Shelf life of carbon nanotube coating in air. An approximate doubling of impedance was seen after one year. This is fully compatible with commercialization. Eight tetrode contacts were measured serially for each graph. Quartiles and extremes are depicted as in Fig. 2. **b**, Impedances of unwanted carbon nanotube crosslinks between individual contacts within a tetrode over time. Crosslinks occur due to overcoating and were largely preventable by ramping of coating currents (Supplementary Fig. 3).

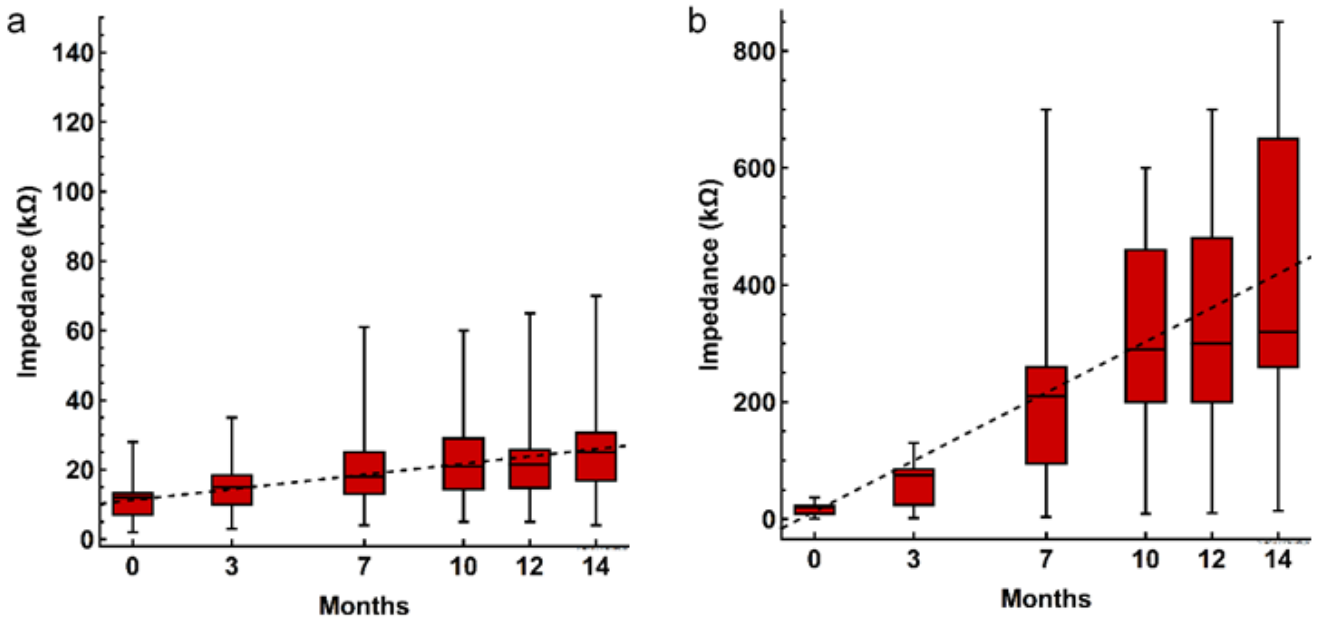

Figure 5 | Large single units recorded over weeks. a, **b**, Stable juxtacellular unit waveforms recorded over weeks in rat substantia nigra pars reticulata (a) and subthalamic nucleus (b). Each red line is a waveform normalized to its mean amplitude for a given day (day 1), with waveforms from all four tetrode channels shown sequentially. The overlay shows that overall waveform shapes are stable over 3 weeks, in each case. The same waveforms are displayed without normalization in Supplementary Fig. 8. **c**, **d**, Waveform shapes are stable over time (days after implantation), as revealed by Pearson correlation coefficients of the data in a and b, relative to the waveform of the first plotted day. The maintenance of overall waveform over weeks of recording suggests that a biological impedance change, rather than a geometric location change of the electrode, was the cause of our minimal drift. **e**, **f**, Waveform peaks and troughs of the same units vary in size over the course of weeks. The maximum and minimum of the data in a and b were plotted as a function of time post implantation. Note that the maximum waveform amplitude reaches well into the mV range. The slow time course of changes suggests a biological process as the cause of waveform drift, rather than mechanical movement of the brain or electrode tip, which would lead to sudden changes in daily recordings. **g**, Large spike amplitudes were recorded from different regions of the rodent brain, including areas not reachable by earlier silicon-based approaches. Black waveforms are 100 superimposed filtered waveforms, extracted randomly from all sorted unit waveforms. Red lines depict the median of these black waveforms.

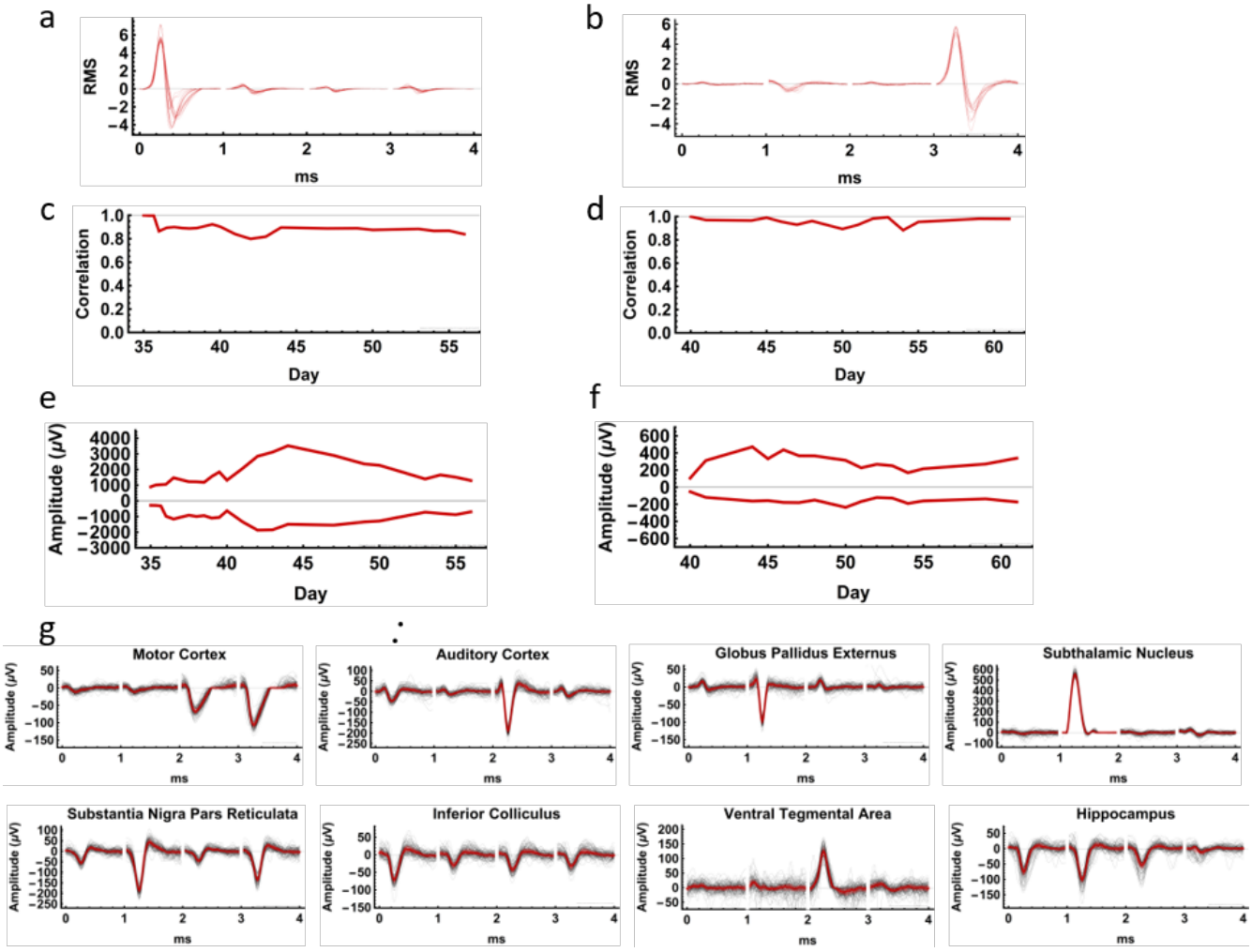

Online Methods

Tetrode Manufacture and Roughening

A base material of platinum 20% iridium wire was used for tetrode manufacture (California Fine Wire Company, USA; teflon coated and stress relieved with 31.75 μm/25 μm shielded/metal diameter). Wires were twisted (without heat curing) and mounted on a custom-designed circuit board to construct an implant with 8 tetrodes (32 recording channels; Fig. 3a-c). The implant included 2 ground wires (bare silver wire Ag-8W, 99.99%, 200μm diameter, Science Products GmbH) that were attached to skull screws, and 2 reference electrodes (teflon-coated silver wire Ag-5T, 99.99%, 125 μm/200 μm metal/coated diameters, balled and chlorided) implanted superficially on neurophysiologically neutral sites such as cerebellum and parietal cortex.

Tetrodes were cut at a 45 degree angle just prior to roughening, using sharp carbide scissors (Fine Science Tools GmbH, Heidelberg Germany). The sharpness of these scissors and the angle of the cut may have a slight effect on final impedances (not significant). Although not systematically tested on large numbers of probes, polishing of tetrode tips provides a smooth surface (Supplementary Fig. 7a) and appears to increase tetrode impedances. Compared to a polished surface, a cut surface (Supplementary Fig. 7b) is microscopically rougher, potentially contributing to the stability of our carbon nanotube coating.

Each tetrode was electrochemically roughened with a protocol modified from previous reports on different metals [36]. First, the cut surface was immersed in 0.5M sulfuric acid solution and roughened by applying a train of square waves at 1 kHz with 50% duty cycle for 60 seconds against a Ag|Ag2SO4 reference electrode. The upper and lower potentials of the square wave were +2.4 V and -0.4 V respectively. The effective duration of roughening time was much shorter than reported previously for platinum [36]. Note that a sonicator was used to prevent gas formation at the tip of tetrodes during roughening and to avoid abnormal oxidation products (Supplementary Fig. 1). Tetrodes were maintained in the sulfuric acid solution at -0.4 V for 3 minutes to reduce oxides prior to rinsing with deionized water and drying.

Carbon nanotube coating

Each tetrode was coated with carbon nanotubes, using a protocol modified from prior reports [37]. The reagents used for CNT coating were as follows: carbon nanotube powder (NC3151, research grade - short thin MWCNT 95+%C purity and surface modified COOH, Nanocyl); poly (sodium 4-styrenesulfate) (average Mw ˜70,000, powder, product #243051, Sigma-Aldrich); pyrrole (reagent grade 98%, product #131709, Sigma-Aldrich).

First, 50 mg of carbon nanotube powder was added to 50 ml of distilled water and placed in a beaker in an ice bath. The carbon nanotube solution was then thoroughly sonicated with a horn sonicator for 45-60 min and transferred to a cylindrical flask. The solution was stirred gently on ice with a magnetic stirrer, while N_2 was gently bubbled to eliminate oxygen from the solution and minimize oxidation. Next, 200mg of poly (Na 4-styrenesulfate) was added and mixed with a magnetic stirrer until dissolved. Finally, 1.736 ml of pyrrole was added. This coating solution provides stable coating results for several hours after pyrrole is added to the preparation.

Eight tetrode tips cut at 45° were immersed in the solution for coating. Prior to coating, these tetrodes were either freshly cut with sharp carbide scissors, or roughened with the procedure outlined above. A voltage of +550 mV for a total coating time of 2100 ms (including linear ramp times of 50 ms) was applied to each electrode. Applying voltage to multiple tetrode contacts simultaneously was avoided, to prevent crosslinking (Supplementary Fig. 3).

Impedance Measurement, Impedance Spectroscopy, and Cyclic Voltammetry

Impedance measurements, impedance spectroscopy, and cyclic voltammetry were conducted independently on several instruments in 3M KCl solution against Ag|AgCl. Standard serial measurements were made at 1 kHz with the Metal Electrode Impedance Tester IMP-1 (Bak Electronics, Umatilla, USA). Impedance spectroscopy was done with nanoZ model 1.2 and nanoZ software version 1.4.0 (White Matter LLC, Seattle USA). Fifteen measurement cycles were acquired at test frequencies from 2Hz to 2kHz. Additional impedance spectroscopy and cyclic voltammetry were performed on a Interface 1010E Potentiostat (Gamry Intruments, Warminster, USA) against a dual-diaphragm Ag|AgCl reference electrode filed with 3M KCl.

Electrode Implantation and Neural Recordings

Electrode implantation in rodents was performed under general anesthesia using 50 mg/kg pentobarbital injected intraperitoneally. Under stereotaxic and physiologic guidance, electrodes were slowly advanced to the target area through a burr hole in the skull using a holder shown in Fig. 3e. Electrodes were cemented at their insertion point to the skull, using UV-curing cyanoacrylate glue (TDS LOCTITE® 4305, Henkel AG & Co. KGaA, Dusseldorf, Germany) and Resilit-S Cold-curing acrylic resin (Erkodent(r) Erich Kopp GmbH, Pfalzgrafenweiler, Germany). Surgical procedures were approved by the state of Saxony-Anhalt, Saxony.

Neural responses were recorded in one adult male macaque monkey under combined isoflurane (0.5-1.0%)/sufentanil citrate (from 0.6 lg/kg/h i.v.) anesthesia in a terminal acute experiment. For details of the set up and procedures, see Ahmed, 2012 39. Housing and husbandry were in compliance with the ARRIVE guidelines of the European Directive (2010/63/EU) for the care and use of laboratory animals. All animal procedures on monkeys were carried out in accordance with Home Office (UK) Regulations and European Union guidelines (EU directive 86/609/EEC; EU Directive 2010/63/EU).

Rodent neural recordings were conducted with Digital Lynx 4SX (Neuralynx, Dublin, Ireland) in a Faraday cage inside an acoustic chamber. Recordings were pre-filtered at 10 to 9000 Hz, and digitized at 14-bits. Rodent recordings were commutated using a custom mechanical swivel (Takagaki et al., in preparation), and rodents were recorded from under freely moving awake-behaving conditions. Some recordings were conducted with an Intan RHD2000 portable system (Intan Technologies, Los Angeles CA, USA) with comparable settings.

Analysis was conducted using Scala/Java (EPFL/Oracle) and Wolfram Mathematica 11.3.0.0 and 12.0 (Wolfram Research, United Kingdom), using block-based modular data stream processing as reported previously [38].

Cell culture, immunocytochemistry, and cell imaging

Primary cultures of rat hippocampal neurons were obtained as previously described [39,40]. After one week in culture on 12 mm glass coverslips, neurons were cultured in the presence of 5 μg/ml carbon nanotubes in the culture medium for 10 days.

Hippocampal neurons were fixed with 4% PFA for 8 mins and then gently incubated with PBS 1X for 2 mins and then with a solution containing 10% horse serum, 0.1 mM glycine, and 0.1% Triton X-100 in Hanks' balanced salt solution two times for 5 min. Pyramidal neurons were morphologically identified based on the side and shape of cell body as observed using anti-MAP2 guinea pig (Synaptic Systems GmbH, Göttingen, Germany; 1:1,000). To visualize synaptic contacts, samples were incubated with rabbit polyclonal synaptophysin 1 (Synaptic Systems; 1:500) for 2 hours at 4°C. Subsequently, samples were incubated with anti-rabbit Cy3-conjugated donkey secondary antibody (1:1,000) for 1 h. Then samples were gently washed and mounted with Mowiol. Fluorescence was visualized using a Zeiss AXIO Imager A2 microscope equipped with a CCD camera (Visitron Systems; camera binning = 1, pixel size = 0.10238 x 0.10238 μm, pixel depth = 16 bytes) using a X63 (1.4 NA) objective.

Acknowledgements

The authors would like to thank Silvia Vieweg and Beate Traore for excellent technical and administrative support. This work was supported by the Leibniz Institute for Neurobiology, DFG Priority Program 1665, the Alexander von Humboldt Foundation, the JMilk Foundation, and the Wellcome Trust (101092/Z/13/Z).

Author contributions

This study was conceived by KT and MTL. Experiments were planned and executed by ZX, KT, GAG, MD, MB, MV, AC, RHM, MTL, and KK. Figures were created by ZX, KT, MD, and MB. Expertise and manuscript writing/editing was provided by KT, ZX, MV, GAG, RHM, MTL, BS, FWO, and KK. Correspondence and material requests should be addressed to KT.

Supplementary Information

Supplementary Figure 1 | Abnormal oxidation products. Prior to optimization of our protocols, abnormal "tree-barking" oxidation products were observed during electrochemical roughening. These oxidation products are presumably due to gas emission and cracking of the substrate metal. Scale bars: 10 μm. **a**, Each contact electrochemically pulsed with square wave potentials at +2.4 V and -0.4 V for 3 minutes, without sonication. **b**, All four contacts were electrochemically pulsed simultaneously for 55 seconds, and kept in 0.5M sulfuric acid solution at -0.4 V for 30 seconds afterwards, without sonication. **c**, Electrochemical pulsing with square wave potentials at +2.4 V and +0.4 V for 3 minutes, without sonication. **d**, Electrochemical pulsing with square wave potentials at -0.4 V and -2.4 V for 3 minutes, without sonication.

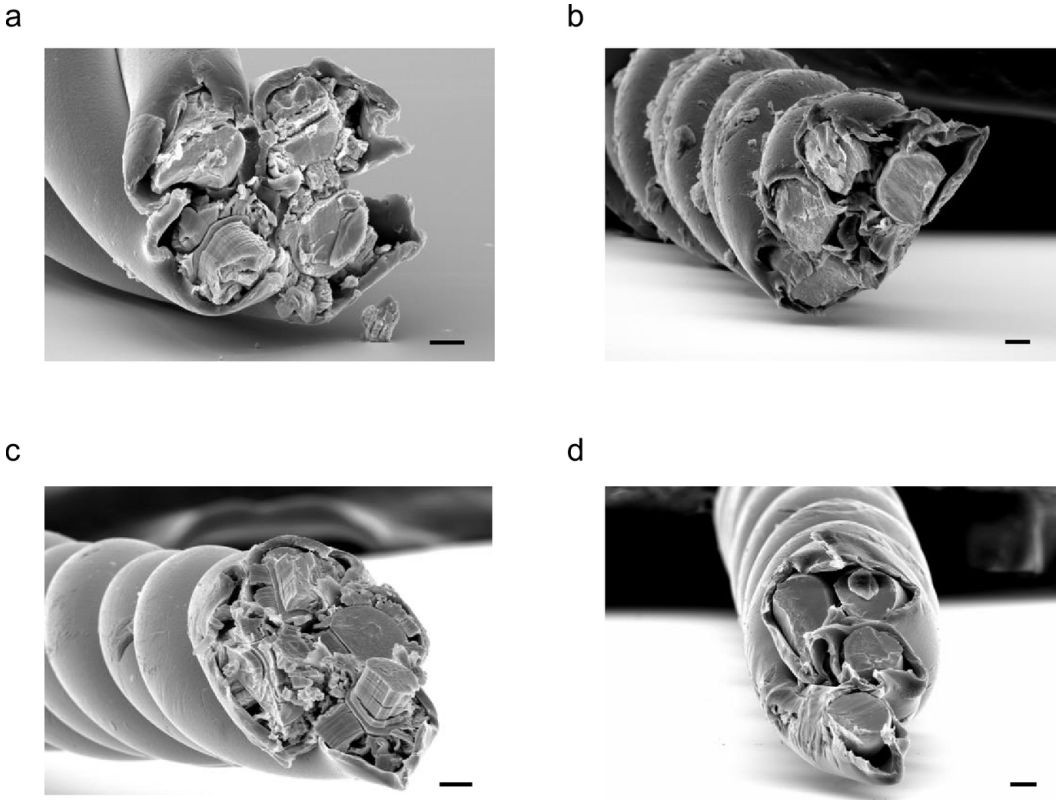

Supplementary Figure 2 | Tetrode impedance drops with roughening time. **a**, The cut surface of a tetrode was immersed and electrochemically roughened in sulfuric acid solution with variable pulsing durations. The approximate log-linear fit indicated by the dotted line (115.934 -54.3555 log10t, t = roughening time in seconds) indicates an exponential process: longer electrochemical roughening results in lower impedance. At roughening times >= 60 s, the impedance decrease saturates at about 8 kOhm. Boxes denote quartiles, horizontal bar is median, whiskers denote most extreme outliers. **b**, Electron micrographs of a tetrode contact after saturated electrochemical roughening (180 s pulsation). Scale bar: 10 µm. **c-h**, Electron micrographs of representative tetrode contacts, after roughening with different pulsation times as plotted in **a**. Scale bars: 10 µm.

Supplementary Figure 3 | Crosslinks due to CNT overcoating. **a**, Crosslinks within a tetrode can be eliminated by applying a high voltage (e.g., approx. 18 V) across the two crosslinked contacts. Empirically, this seemed to increase the incidence of carbon nanotubes falling off during or after implantation (Supplementary Table 5). Scale bar: 10 μm. **b-d**, Ramping of coating current prevents crosslinking. **b**, Sample coating currents without ramp. When coating each tetrode contact sequentially, the 2nd, 3rd, and 4th contacts (coded by increasingly darker colors) often show an initial current flow when voltage is applied, indicating lower starting impedance with subsequent contacts. This demonstrates that coating of previous contacts affects subsequent contacts, which may be due to capacitive currents leading to poorly controlled CNT coating and crosslinks at non-targeted contacts. **c**, Sample coating currents with 50 ms ramp added to applied voltage. Adding a ramp prevents crosslinks almost completely, and initial capacitive currents are not seen. **d**, Sample coating currents for CNT coating of a roughened tetrode. All traces have high initial capacitive currents, due to the higher capacitance of roughened contacts, but the high capacitance did not lead to spurious crosslinking.

Supplementary Figure 4 | Impedance Spectroscopy. Electrodes with the four types of surface processing (cut/untreated, [?]; coated with carbon nanotubes, C; electrochemically roughened, R; electrochemically roughened and CNT coated, R+C) show log-linear reduction in impedance over frequency, as expected from a mostly capacitive electrode interface. While cut and roughened electrodes show the highest impedances, coated as well as roughened and coated electrodes have low impedances optimal for high signal-to-noise recordings of neuronal signals.

Supplementary Table 5 | Coating failure during the first week of implantation. Loss of carbon nanotube (CNT) coating in single channels of a tetrode occurs exclusively during the first week after successful implantation. It is likely that active biological processes such as glial phagocytosis are involved.

Supplementary Figure 6 | Loss of carbon nanotube coating during implantation. Recording during implantation with a carbon nanotube coated tetrode. Sudden increase of baseline noise was observed on one channel, which may be due to either loss of carbon nanotube coating or disrupted contact between carbon nanotubes and metal surface. In contrast to the loss of carbon nanotube coating, channels with intact coating show low baseline noise on the recorded signal. Note that our high capacitance electrode interface in coated channels also allows simultaneous recording of slow and fast local field potentials (LFP). Such LFP are useful for measuring population activity brain states associated with sleep and attention.

Supplementary Figure 7 | Polishing of tetrode tips. **a**, Tetrode tip polished with a circular grinder to 90 degrees after cutting. **b**, Tetrode tip cut with sharp carbide scissors at 45 degrees. Empirically, the polished tetrodes did not perform better than cut tetrodes. We believe that the macroscopic surface roughness of the cut surface may be contributing to carbon nanotube adhesion. Scale bar: 10 μm.

Supplementary Figure 8 | Single units can be recorded over weeks in multiple brain areas. Daily cluster waveforms of data shown in Fig. 5. **a** corresponds to panels a, c, and e in Fig. 5. **b** corresponds to panels b, d, and f in Fig.5.

Supplementary Figure 9 | Cell morphology and synaptic contacts in neuronal cultures exposed to carbon nanotubes. After long-term incubation with carbon nanotubes (see Methods), hippocampal neurons were fixed and stained with an antibody against the presynaptic marker synaptophysin 1 (red) at 17 days in vitro. Intact cell morphology and the presence of dark precipitates of carbon nanotube were confirmed under combined brightfield-fluorescent illumination. Scale bar: 10 μm. Note that despite direct contact of several carbon nanotubes, dendrites developed normally. Synapse number and fluorescent puncta size are grossly normal. Such nanointerfaces such as carbon nanotubes are known to support biocompatibility and biocontact [41,42,43].

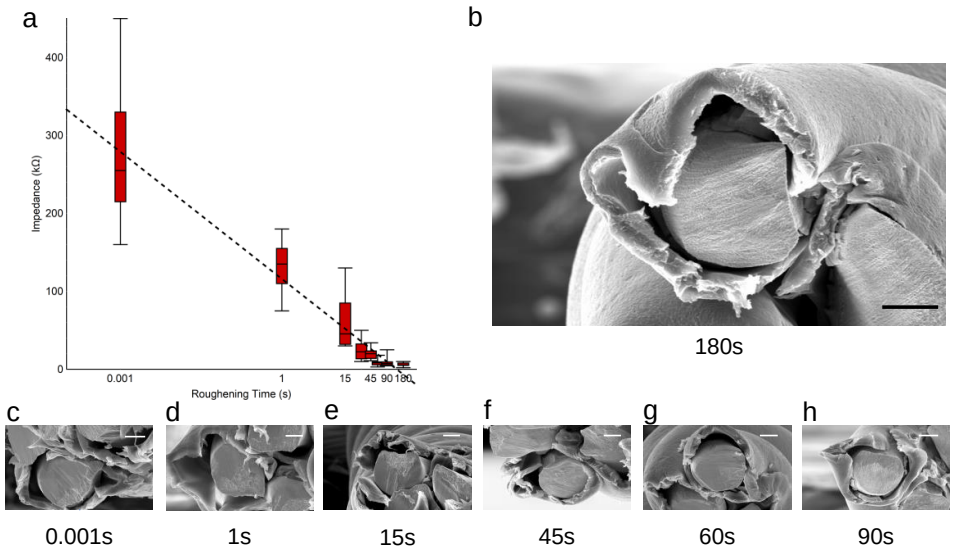
a
b
400
300
200
100
0
Impedance (kΩ)
0.001
1
15
45
90
180
Roughening Time (s)
180s
c
d
e
f
g
h
0.001s
1s
15s
45s
60s
90s

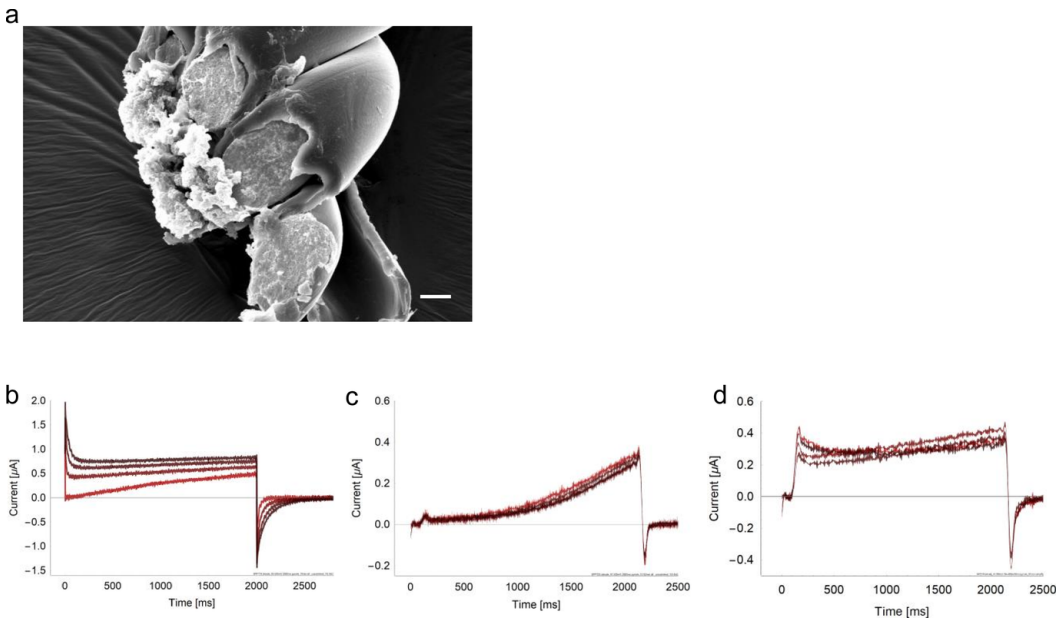
a
b
c
d
Current [µA]
Time [ms]

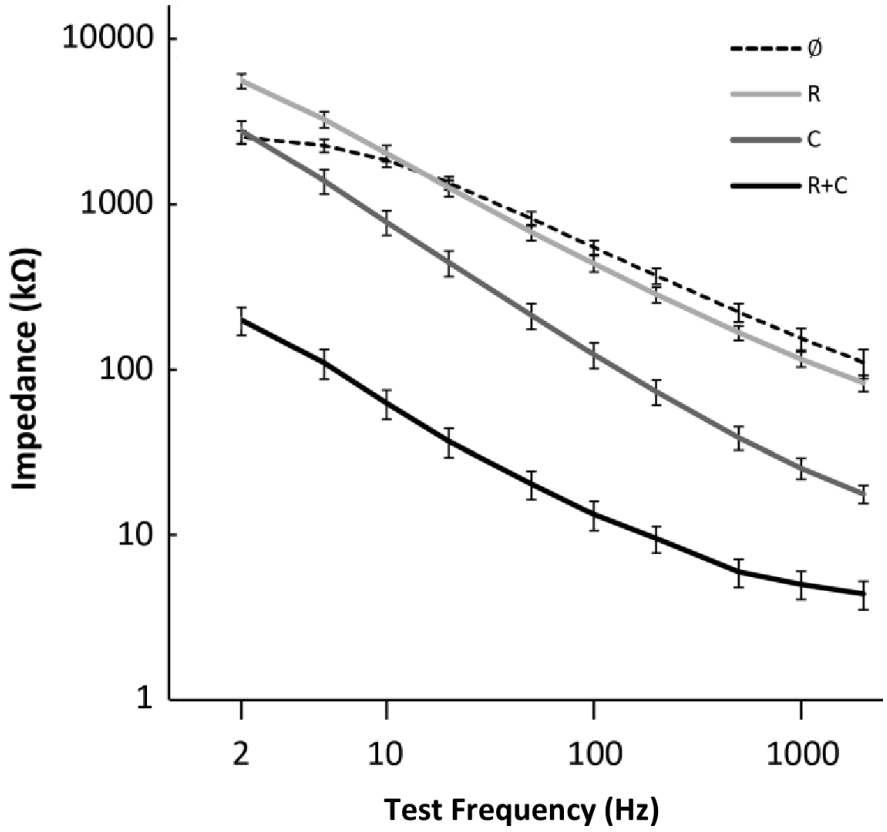
Ø
R
C
R+C
Impedance (kΩ)
Test Frequency (Hz)

Supplementary Table 5 | Chances of CNT loss during or within one week after implantation	
	Total number of contacts
CNT coating	3.30% (39/1182)
Roughening & CNT coating	0.34% (2/587)

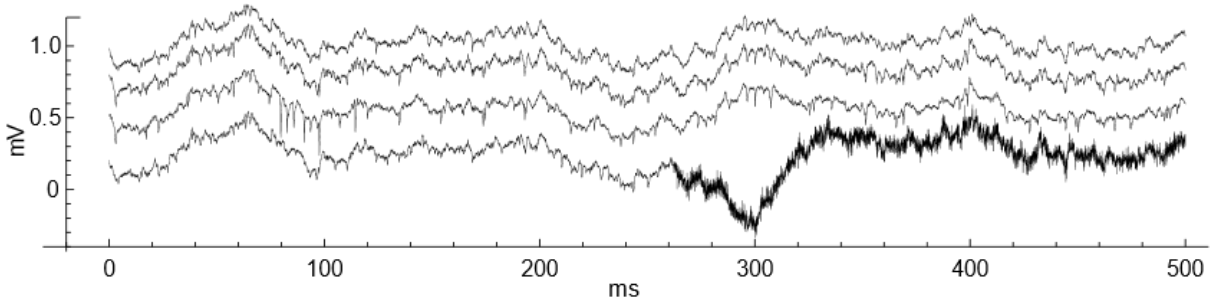

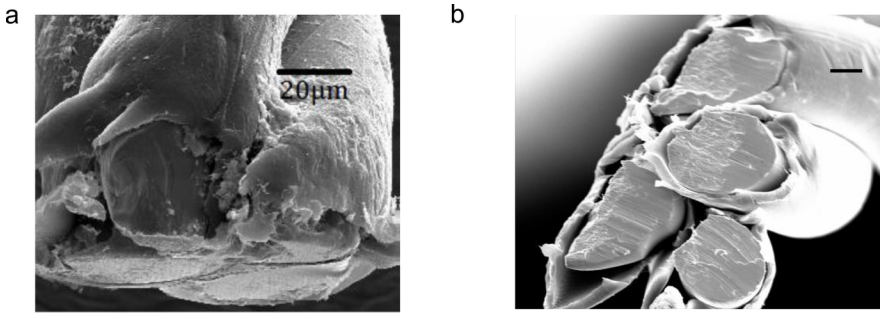

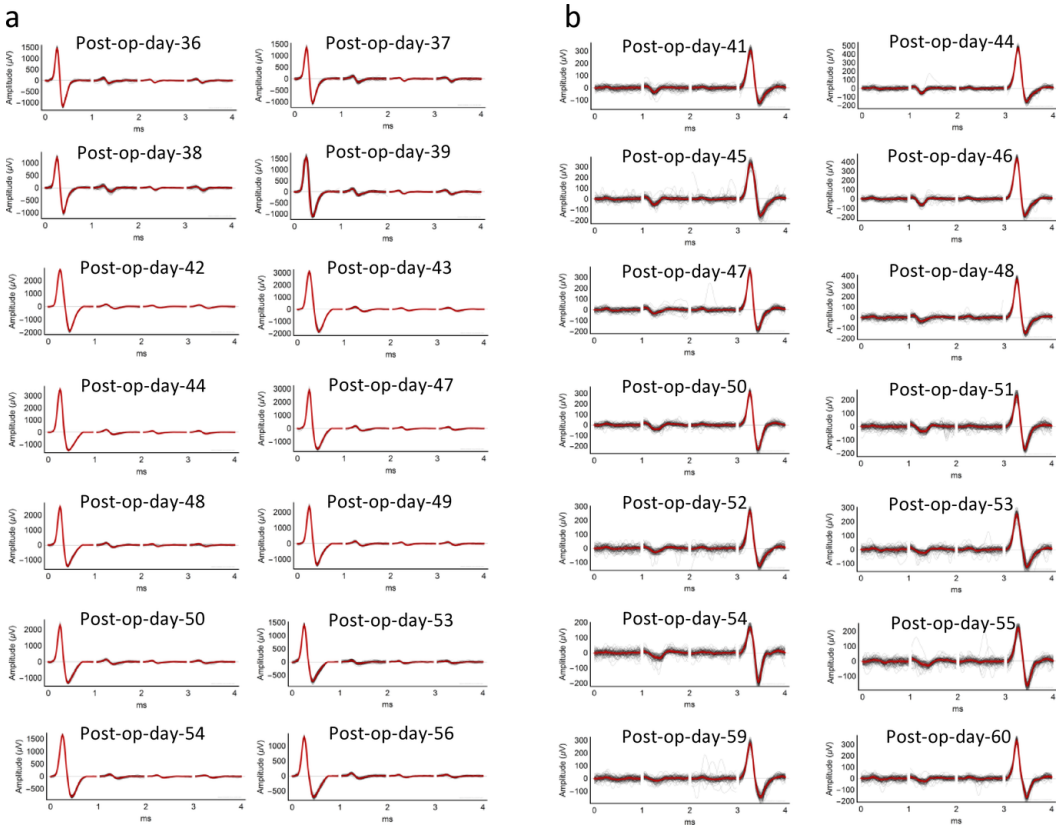
a
Post-op-day-36
Post-op-day-37
Post-op-day-38
Post-op-day-39
Post-op-day-42
Post-op-day-43
Post-op-day-44
Post-op-day-47
Post-op-day-48
Post-op-day-49
Post-op-day-50
Post-op-day-53
Post-op-day-54
Post-op-day-56
b
Post-op-day-41
Post-op-day-44
Post-op-day-45
Post-op-day-46
Post-op-day-47
Post-op-day-48
Post-op-day-50
Post-op-day-51
Post-op-day-52
Post-op-day-53
Post-op-day-54
Post-op-day-55
Post-op-day-59
Post-op-day-60

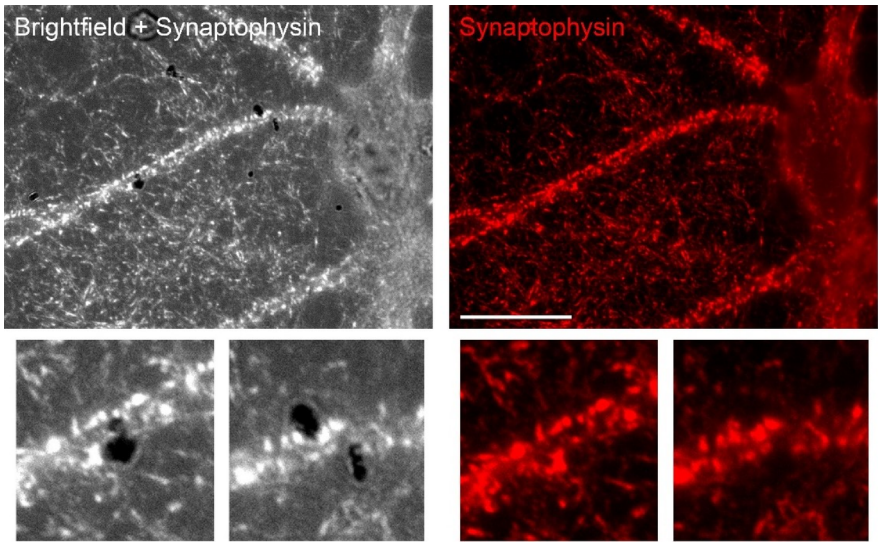
Brightfield + Synaptophysin
Synaptophysin

References

1.Ghane-Motlagh, B. & Sawan, M. Design and Implementation Challenges of Microelectrode Arrays: A Review. *Materials Sciences and Applications* **04**, 483–495 (2013).

2.Chapin, J. K. Using multi-neuron population recordings for neural prosthetics. *Nature Neuroscience* **7**, 452–455 (2004).

3.Krüger, J., Caruana, F., Volta, R. D. & Rizzolatti, G. Seven years of recording from monkey cortex with a chronically implanted multiple microelectrode. *Front Neuroeng* **3**, 6 (2010).

4.McMahon, D. B., Jones, A. P., Bondar, I. V. & Leopold, D. A. Face-selective neurons maintain consistent visual responses across months.. *Proc Natl Acad Sci U S A* **111**, 8251–6 (2014).

5.Guan, S. *et al.*. Elastocapillary self-assembled neurotassels for stable neural activity recordings.. *Sci Adv* **5**, eaav2842 (2019).

6.Luan, L. *et al.*. Ultraflexible nanoelectronic probes form reliable, glial scar-free neural integration.. *Sci Adv* **3**, e1601966 (2017).

7.Fu, T. M., Hong, G., Viveros, R. D., Zhou, T. & Lieber, C. M. Highly scalable multichannel mesh electronics for stable chronic brain electrophysiology.. *Proc Natl Acad Sci U S A* **114**, E10046–E10055 (2017).

8.Normann, R. A., Maynard, E. M., Rousche, P. J. & Warren, D. J. A neural interface for a cortical vision prosthesis. *Vision Research* **39**, 2577–2587 (1999).

9.Bhandari, R., Negi, S. & Solzbacher, F. Wafer-scale fabrication of penetrating neural microelectrode arrays. *Biomedical Microdevices* **12**, 797–807 (2010).

10.Rousche, P. J. & Normann, R. A. Chronic recording capability of the Utah Intracortical Electrode Array in cat sensory cortex.. *J Neurosci Methods* **82**, 1–15 (1998).

11.Bridges, A. W. *et al.*. Chronic inflammatory responses to microgel-based implant coatings. *Journal of Biomedical Materials Research Part A* **94A**, 252–258 (2010).

12.Anderson, J. M. Inflammatory Response to Implants. *ASAIO Journal* **34**, 101–107 (1988).

13.Coleman, D. L., King, R. N. & Andrade, J. D. The foreign body reaction: A chronic inflammatory response. *Journal of Biomedical Materials Research* **8**, 199–211 (1974).

14.Anderson, J. M. & Jiang, S. Implications of the Acute and Chronic Inflammatory Response and the Foreign Body Reaction to the Immune Response of Implanted Biomaterials. in *The Immune Response to Implanted Materials and Devices* 15–36 (Springer International Publishing, 2016). doi:10.1007/978-3-319-45433-7_2.

15.Gray, C. M., Maldonado, P. E., Wilson, M. & McNaughton, B. Tetrodes markedly improve the reliability and yield of multiple single-unit isolation from multi-unit recordings in cat striate cortex. *Journal of Neuroscience Methods* **63**, 43–54 (1995).

16.Buzsáki, G. Large-scale recording of neuronal ensembles.. *Nat Neurosci* **7**, 446–51 (2004).

17.Tolias, A. S. *et al.*. Recording chronically from the same neurons in awake, behaving primates.. *J Neurophysiol* **98**, 3780–90 (2007).

18.Jun, J. J. *et al.*. Fully integrated silicon probes for high-density recording of neural activity.. *Nature* **551**, 232–236 (2017).

19.Cheung, K. C., Renaud, P., Tanila, H. & Djupsund, K. Flexible polyimide microelectrode array for in vivo recordings and current source density analysis. *Biosensors and Bioelectronics* **22**, 1783–1790 (2007).

20.Fries, P. & Lewis, C. Set for applying a flat, flexible two-dimensional thin-film strip into living tissue. *United States Patent and Trademark Office* **US20170181707A1**, (2015).

21.Chung, J. E. *et al.*. High-Density Long-Lasting, and Multi-region Electrophysiological Recordings Using Polymer Electrode Arrays. *Neuron* **101**, 21–31.e5 (2019).

22.Musk, E. & Neuralink. An integrated brain-machine interface platform with thousands of channels. *BioRxiv* (2019) doi:10.1101/703801.

23.Yang, X. *et al.*. Bioinspired neuron-like electronics. *Nature Materials* **18**, 510–517 (2019).

24.Deepthi, R., Bhargavi, R., Jagadeesh, K. & Vijaya, M. S. Rheometric Studies on Agarose Gel- A Brain Mimic Material. *SASTech Journal* **9**, (2010).

25.Cui, X. & Martin, D. C. Fuzzy gold electrodes for lowering impedance and improving adhesion with electrodeposited conducting polymer films. *Sensors and Actuators A: Physical* **103**, 384–394 (2003).

26.Ferguson, J. E., Boldt, C. & Redish, A. D. Creating low-impedance tetrodes by electroplating with additives. *Sensors and Actuators A: Physical* **156**, 388–393 (2009).

27.Keefer, E. W., Botterman, B. R., Romero, M. I., Rossi, A. F. & Gross, G. W. Carbon nanotube coating improves neuronal recordings. *Nature Nanotechnology* **3**, 434–439 (2008).

28.Ludwig, K. A. *et al.*. Poly(3,4-ethylenedioxythiophene) (PEDOT) polymer coatings facilitate smaller neural recording electrodes. *Journal of Neural Engineering* **8**, 014001 (2011).

29.Geddes, L. A. *Electrodes and the measurement of bioelectric events.* (Wiley-Interscience, 1972).

30.Williams, J. C., Rennaker, R. L. & Kipke, D. R. Stability of chronic multichannel neural recordings: Implications for a long-term neural interface. *Neurocomputing* **26-27**, 1069–1076 (1999).

31.Dhawale, A. K. *et al.*. Automated long-term recording and analysis of neural activity in behaving animals. *eLife* **6**, (2017).

32.Moore, J. J. *et al.*. Dynamics of cortical dendritic membrane potential and spikes in freely behaving rats. *Science* **355**, (2017).

33.Bareket-Keren, L. & Hanein, Y. Carbon nanotube-based multi electrode arrays for neuronal interfacing: progress and prospects. *Frontiers in Neural Circuits* **6**, (2013).

34.Dickey, A. S., Suminski, A., Amit, Y. & Hatsopoulos, N. G. Single-Unit Stability Using Chronically Implanted Multielectrode Arrays. *Journal of Neurophysiology* **102**, 1331–1339 (2009).

35.Pinault, D. A novel single-cell staining procedure performed in vivo under electrophysiological control: morpho-functional features of juxtacellularly labeled thalamic cells and other central neurons with biocytin or Neurobiotin. *Journal of Neuroscience Methods* **65**, 113–136 (1996).

36.Weremfo, A., Carter, P., Hibbert, D. B. & Zhao, C. Investigating the Interfacial Properties of Electrochemically Roughened Platinum Electrodes for Neural Stimulation. *Langmuir* **31**, 2593–2599 (2015).

37.Keefer, E. W., Botterman, B. R., Romero, M. I., Rossi, A. F. & Gross, G. W. Carbon nanotube coating improves neuronal recordings. *Nature Nanotechnology* **3**, 434–439 (2008).

38.Takagaki, K., Zhang, C., Wu, J. Y. & Ohl, F. W. Flow detection of propagating waves with temporospatial correlation of activity. *J Neurosci Methods* **200**, 207–18 (2011).

39.Herrera-Molina, R. *et al.*. Structure of excitatory synapses and GABAA receptor localization at inhibitory synapses are regulated by neuroplastin-65.. *J Biol Chem* **289**, 8973–88 (2014).

40.Herrera-Molina, R. & von, B. R. Transforming growth factor-beta 1 produced by hippocampal cells modulates microglial reactivity in culture.. *Neurobiol Dis* **19**, 229–36 (2005).

41.Posati, T. *et al.*. A Nanoscale Interface Promoting Molecular and Functional Differentiation of Neural Cells.. *Sci Rep* **6**, 31226 (2016).

42.Guitchounts, G., Markowitz, J. E., Liberti, W. A. & Gardner, T. J. A carbon-fiber electrode array for long-term neural recording.. *J Neural Eng* **10**, 046016 (2013).

43.Patel, P. R. *et al.*. Chronic in vivo stability assessment of carbon fiber microelectrode arrays.. *J Neural Eng* **13**, 066002 (2016).